frontiers | Frontiers in Energy Research

TYPE Original Research
PUBLISHED 11 August 2023
DOI 10.3389/fenrg.2023.1219664

OPEN ACCESS

EDITED BY
Lin Tiejun,
Southwest Petroleum University, China

REVIEWED BY
Chengyuan Xu,
Southwest Petroleum University, China
Jinze Xu,
University of Calgary, Canada
Hongjian Zhu,
Yanshan University, China
Qigui Tan,
Changzhou University, China

*CORRESPONDENCE
Zhangming Hu,
huzhmkl@cnpc.com.cn

RECEIVED 09 May 2023
ACCEPTED 21 July 2023
PUBLISHED 11 August 2023

CITATION
Hu Z, Hu M, Xiong X, Zheng L, Wu N, Guang Y, Hu X and Huang X (2023), Geochemical characteristics of the braided river reservoir in block 19 of the sulige gas field.
Front. Energy Res. 11:1219664.
doi: 10.3389/fenrg.2023.1219664

Geochemical characteristics of the braided river reservoir in block 19 of the sulige gas field

Zhangming Hu[1,2]*, Mingyi Hu[1,3], Xianyue Xiong[4], Lijun Zheng[2], Nan Wu[1,3], Youhui Guang[2], Xiaoling Hu[2] and Xin Huang[1,3]

[1]School of Earth Sciences, Yangtze University, Wuhan, Hubei, China, [2]Geological Research Institute of CNPC Xibu Drilling Engineering Company Limited, Kramay, Xinjiang, China, [3]Hubei Cooperative Innovation Center of Unconventional Oil and Gas, Yangtze University, Wuhan, Hubei, China, [4]PetroChina Coalbed Methane Company Limited, Beijing, China

The sand body structure and geochemical characteristics of braided river reservoirs are the key geological factors affecting gas production and development effects. The Sulige gas field in the Ordos Basin is an important large-scale gas-producing layer. Owing to the control of sedimentary facies, the geological structure of the sand body changes greatly and its connectivity is poor. The geological characteristics have not yet been elucidated, and this is an important problem restricting the development of the Sulige Gas Field. To solve this problem, this study focuses on the braided river reservoir of the Shihezi Formation in Block 19 of the Sulige Gas Field, conducts geological surveys in the study area, analyzes the geological and geochemical characteristics of the reservoir, and obtains samples through drilling. Through a thin-section test, gas-water two-phase experiment, and simulation test, the braided river reservoir configuration and pore and gas-water characteristics are obtained. The results show that the reservoir lithology in the study area is mainly composed of quartz sandstone, lithic sandstone, and quartzy lithic sandstone, with a porosity of 3%–13% and a permeability of $(0.05–0.7) \times 10^{-3}$ m^2. The reservoir has low porosity and low permeability. After drilling samples were obtained, 32 thin-section rock samples were selected. The pore types of the block reservoir mainly (82.9%) consisted of intragranular and intergranular dissolved pores. The difference in pore structure was mainly reflected by the size and distribution of the throat. The distribution of physical properties was 6%–10%, the gas saturation was 61%, the NMR effective porosity was 7.49%, the permeability was 4.08×10^2 μm^2, and the physical properties were relatively good. In terms of the study area, the average thickness of the single braided channel in the lower section of He 8 was 4.7 m, the average width of the channel was 963 m, and the composite channel was distributed in a potato shape, parallel to the direction of the main flow. The average length of the channel was 2,147 m and the average width was 844 m. As the porosity increased, the efficiency of gas-driven water also increased, and there was a linear positive correlation between porosity and gas-driven water efficiency. With the increase in movable water saturation, the water-air ratio became larger and water production was greater. In low-amplitude structures and under low-permeability background conditions, for reservoirs with good local pore structure and physical properties, the water remaining at the bottom of the reservoir or sand body was controlled by the accumulation conditions or the weak structural differentiation after accumulation. In terms of the gas and water produced simultaneously in the study area, gas production was less than 2×10^4 m^3/d and water production was relatively large at more than

10 m^3/d; gas and water were mainly distributed in the downdip part of the main channel structure or in the island lens-shaped permeable sand bodies trapped by the surrounding tight layers. The study results provide theoretical data support for the exploration and production of the Sulige Gas Field.

KEYWORDS

braided river reservoir, geological characteristics, sulige gas field, characteristics of reservoir rock mass, sand body distribution

1 Introduction

Natural gas, as a clean, efficient, and versatile fossil fuel, can provide reliable energy support for industries, power generation, heating, and other fields. The importance of fracturing technology in natural gas exploitation is that it can effectively release natural gas and improve natural gas productivity in the reservoir and promote the development of unconventional gas fields, such as shale gas. The Lower Shihezi Formation of Middle Permian in the Ordos Basin is a high-yield tight sandstone gas reservoir dominated by lithologic traps in the Upper Paleozoic; the Sulige gas field, located in the northeast margin of the Ordos Basin, has become the largest integrated natural gas field (Yang et al., 2008). Development of the Sulige gas field is mainly constrained by complex geological conditions, including the deep burial of gas reservoirs, high sulfur compounds, and dense reservoirs, which are technically difficult to overcome and have high investment costs. Therefore, this study on the geology of braided river reservoirs is helpful for subsequent mining. This study mainly discusses the chemical characteristics of its reservoirs in terms of geological conditions. The formation and distribution mechanism of sand bodies in the He-8 member of the Sulige gas field is influenced by a sedimentary facies belt. The lower member of He-8 is a braided river sedimentary reservoir, and the thickness and properties of its reservoir sand bodies change greatly and the continuity is poor, which leads to the unclear distribution law of sand bodies, thus affecting the deployment of production wells and natural gas exploitation (Zhu et al., 2021). Therefore, the geochemical characteristics of the braided river sand body reservoir in the lower member of He 8 in the Sulige gas field in the Ordos Basin is an important research topic.

A lot of research has been carried out on braided river sand body reservoirs. Braided river reservoirs are characterized by a small distribution range of a single sand body, mudstone interlayer development, and the overlapping of multiple sand bodies, and at the same time, interlayer and multigenetic seepage barriers lead to poor sand body connectivity (Li et al., 2021). Some researchers believe that braided rivers mostly develop in mountainous areas, and the change of river channels leads to the interconnection of multiple sand bodies in vertical and lateral directions, forming widely distributed thick sandstone. The types of sand bodies are beach bar and river filling, and there are many interconnected beach-bar sand bodies embedded in the valley. Braided river sand bodies are wide and shallow and characterized by multiple rivers, large riverbed gradients, rapid lateral migration, and microfacies, such as braided rivers, beach bars, abandoned rivers, and flood plains (Zhu et al., 2022). Some researchers have carried out simulations of braided river sediment outcrops and river sediments and determined whether they belong to the same beach-bar sand body by identifying the single wells of two adjacent wells and judging whether they belong to a single beach-bar sand body using dynamic and static data, and determined that the longitudinal sand bar is the main body of the beach. Some researchers discussed the division between the beach bar and channel-filling microfacies through core observation and analysis, curve logging, and mud logging, followed by a comparison with similar outcrop deposits. At the same time, they carried out single-well identification and cross-well comparison of the silting layer in the braided beach-bar sand body, carefully dissected the reservoir sand body and its internal configuration, and summarized the structural deposition model of braided river sand bodies characterized by "flat forward accumulation of the beach bar downstream and vertical multi-stage accretion". To study the sedimentary model of a braided river in depth, some researchers have established the sedimentary model of a braided river rich in sand and mud and summarized the sedimentary model of the braided river using the concepts of lithofacies and lithofacies combination, while comprehensively considering the geological characteristics, geographical background, and climate characteristics of braided river development. Some researchers use a gravelly braided river as the research object, which proves that there are many sedimentary microfacies in braided rivers, and the microfacies units and microfacies are also very complex. Other researchers have studied the influence of river location on braided river development and found that when certain braided conditions are met, the river pattern may be transformed. Through careful investigation of cores, some researchers have summarized the main sedimentary characteristics of braided river deposits by comprehensively analyzing thin-section identification, logging, and test data and identified large-scale hierarchical interfaces and hierarchical entities according to river hierarchy classification; they then further identified small-scale hierarchical interfaces and hierarchical entities internally. According to sedimentary structure, sequence characteristics, and logging profiles, some researchers have analyzed the temporal and spatial distribution and variation law of braided river sedimentary facies. Braided river and interbank sand bars are mainly glutenite and medium-coarse sandstone. Some researchers used dense well-pattern logging, sedimentation, and physical property analysis to analyze the hierarchical types and scales of reservoir sand bodies. By comparing the filling styles and quantitative scales of braided rivers and Xintanba, according to the structural elements and geometric characteristics of braided river sand bodies, the geological knowledge base of braided river reservoirs was constructed. Additionally, researchers have analyzed the formation and evolution process of the beach sand dam and braided channel from a dynamic point of view and focused on

FIGURE 1
Reservoir lithology in the study area.

the differences among the existing states of the three channels: active channel, sandy channel filling, and abandoned channel filling.

In this study, the braided river reservoir in the eighth member of the Hetable Formation in Block 19 of the Sulige gas field is used as the research object, and the geological and geochemical characteristics of the reservoir are analyzed through geological investigation in the research area. Through drilling sampling, thin-section tests, gas-water two-phase experiments, and simulation tests, the braided river reservoir configuration, porosity, and gas-water characteristics are obtained, providing theoretical data support for the exploration and production of the Sulige gas field.

2 Geological background of the study area

2.1 Geological survey

The Ordos Basin is located in the western North China platform, and its stratigraphic structure is divided into six structural units: the Yishan slope, Yimeng uplift, Weibei uplift, Shanxi flexure belt, Tianhuan depression, and western margin thrust belt. The Sulige gas field is located in the northwest of the Ordos Basin, which belongs to the second-order structural unit of the Yishan slope. The stratum is a gentle monocline with a westward dip and no fault development. Block 19 of the Sulige gas field is located in the third phase of the western part of the Sulige gas field, with an area of over 1,400 km^2, a prospecting area of approximately 750 km^2, an average reserve abundance coefficient of 1.15 × 108 m^3/km^2, and a composite channel width of 10 km in the east. The internal structure is relatively complex, the sand body scale is small but changes rapidly, and the heterogeneity is strong, making it difficult to drill. At the same time, the reservoir has a water content and gas-water relationship in some areas. Figure 1 shows the reservoir lithology in the study area, and Table 1 shows the reservoir rock mass characteristics in the study area. Sandstone reservoirs in the study area are mainly distributed in the Lower Jurassic Manasi River Formation and Cretaceous optional intervals. The Lower Jurassic Manasi River Formation is the main sandstone reservoir in the study area, while the Cretaceous optional intervals are distributed in the upper Cretaceous Tarim Formation, alkali spring formation, and other strata, including sandstone, limestone, and mudstone reservoirs. However, the distribution of sandstone reservoirs in the study area is uneven, and there are certain differences in the characteristics and advantages of sandstone reservoirs. This requires developers to fully investigate before formulating corresponding development strategies. The lithology of the lower member of He 8 is mainly quartz sandstone, lithic sandstone, and quartz lithic sandstone, with porosity mainly distributed in 3%–13% of this lithology and permeability mainly distributed in (0.05–0.7) × 10^{-3} μm^2, belonging to a low-porosity and low-permeability reservoir.

2.2 Geological survey

According to the field outcrop profile in the eastern margin of the Ordos Basin, it is characterized by the complete development of sedimentary sequences from the Paleozoic to the Cenozoic, diverse sedimentary environments, and frequent changes (Zhu et al., 2018). The climate in this area is dry, and the vegetation is not well developed. The interlayer water in the Ordos Basin is developmentally characterized by a widespread distribution, high salinity, relatively high pressure, and good permeability, which have a significant impact on the formation and storage of oil and gas reservoirs (Li et al., 2019). The outcrop of the lower member of He 8 is complete, and it is obvious in vertical and oblique paleocurrents. The strata are gentle and extend far away, and the lithofacies combination and spatial superposition style are clearly visible. According to the characteristics of lithology, lithofacies, and sedimentary cycle, the member of He 8 can be divided into two lower layers, one lower layer, two upper layers, and one upper layer from bottom to top. The lower member of He 8 is a sandy braided river deposit, and the upper member is braided river to meandering river deposit.

2.3 Reservoir petrophysical characteristics

Through drilling sampling and the observation of 32 rock thin slices, it was found that the reservoir mainly contains quartz

TABLE 1 Characteristics of reservoir rock mass in the study area.

Rock character	Porosity (%)	Permeability (μm^2)	Deposition thickness (m)
Malmstone	3–13	(0.05–0.7) × 10^{-3}	40

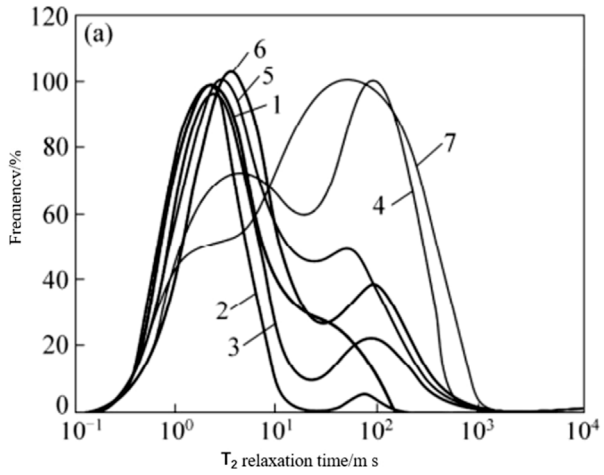

FIGURE 2
Contrast in T_2 spectrum distribution of the He 8 reservoir in the east of the Sulige gas field.

minerals, which promotes the development of the physical properties of the reservoir, and the content of cuttings and interstitial materials destroy the physical properties of the reservoir. Sedimentary microfacies, such as distributary channels and flood plains, are mainly developed in the study area, where coarse-grained quartz sandstone has developed in the middle of the distributary channel, which is a favorable place to form relatively high permeability reservoirs. The pore types of block reservoirs are mainly (82.9%) intragranular and intergranular dissolved pores; diagenesis is dense, intergranular pores are less developed, and the remaining intergranular pores make up the remaining 9.1%. There are a few micro-cracks in the study area, and the area ratio is positively correlated with physical properties.

The pore radius curves with different permeabilities are basically the same and the distribution is relatively concentrated. With the change of permeability, the peak value and distribution range of the throat radii are different. The difference in pore structure is mainly reflected in the size and distribution of the throat. Figure 2 shows the nuclear magnetic resonance T_2 spectrum of He 8. The porosity of He 8 shows double peak characteristics and movable fluid porosity development.

The T_2 spectrum of He 8 shows two peaks, with well-developed movable pores and well-developed pores in the cast sheet, with a physical property distribution of 6%–10% and a gas saturation of 61%. The He-8 member is widely distributed on the T_2 spectrum of nuclear magnetic resonance, with a high peak and a certain difference spectrum oil and gas signal, which is gas bearing. From the perspective of nuclear magnetic pore structure, small and medium pores are mainly present, with an effective nuclear magnetic porosity of 7.49% and a permeability of 0.408 × 10^3 μm^2, with relatively good physical properties. The array acoustic wave indicates gas; according to the conventional logging curve, three pores have an envelope surface, which is comprehensively interpreted as a gas reservoir.

3 Reservoir geochemical characteristics

3.1 Anatomy of the reservoir configuration

Through outcrop observation, the main microfacies of the He 8 member are a braided channel and a heart beach. Figure 3 shows the division of sedimentary microfacies of the braided river, which is mainly divided into three subfacies: a braided channel, an overflow bank, and a flood plain. Braided channel subfacies can be divided into two microfacies: beach and braided channel. Overflow bank subfacies can be divided into three microfacies: an inter-channel, a natural breakwater, and a crevasse fan (Caili et al., 2021). Because the overbank deposits are not developed in the process of the frequent swinging of the braided channel, the research on braided river reservoir configuration focuses on the beach and braided channel (Lu et al., 2015). The braided river water inventory faces challenges in reservoir prediction and exploration

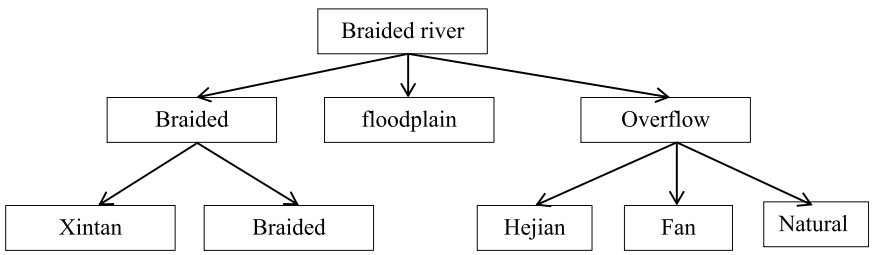

FIGURE 3
Sedimentary microfacies division of the braided river.

10.3389/fenrg.2023.1219664

TABLE 2 Single braided channel and maximum sand body thickness.

Layer	River channel	Sand body width (m)	Sand layer thickness (m)	Flakiness ratio	Layer	River channel	Sand body width (m)	Sand layer thickness (m)	Flakiness ratio
He 8 lower 1_1	①	966	3.1	315	He 8 Lower 2 1	⑥	1,094	3.1	355
	②	839	4.0	209		⑦	1,343	3.9	346
	③	1,182	4.6	255		⑧	1,245	4.5	277
He 8 lower 1_2	①	2,113	4.6	456		⑨	885	1.9	455
	②	968	4.5	215		⑩	377	2.0	186
	③	920	4.8	190		⑪	1,160	3.3	353
	④	1,381	3.2	431		⑫	918	4.7	196
	⑤	795	4.1	193		⑬	1,171	4.5	257
	⑥	1,084	3.7	293	He 8 Lower 2_2	①	830	6.2	133
	⑦	956	4.0	240		②	1,095	6.1	180
	⑧	701	1.0	677		③	932	6.4	145
	⑨	789	4.5	177		④	1,087	6.8	159
	⑩	776	5.2	149		⑤	1,167	5.9	196
He 8 lower 1_3	①	759	4.7	161		⑥	1,005	3.8	265
	②	816	4.5	180		⑦	884	5.7	156
	③	869	6.1	143		⑧	845	5.7	147
	④	1,103	4.3	255		⑨	925	8.0	116
	⑤	1,026	4.3	236		⑩	867	3.9	223
	⑥	767	4.3	178		⑪	938	6.0	157
	⑦	780	5.0	156		⑫	1,163	5.4	214
	⑧	906	5.8	155	He 8 Lower 2_3	①	1,153	3.5	329
	⑨	1,166	4.0	291		②	983	5.8	170
	⑩	868	5.3	165		③	788	3.7	212
	⑪	769	6.3	123		④	848	4.3	195
	⑫	805	3.7	215		⑤	834	4.5	186
	⑬	1,193	2.7	434		⑥	756	4.3	176
	⑭	807	5.7	141		⑦	713	4.3	165
He 8 lower 2_1	①	728	3.2	225		⑧	1,341	5.9	228
	②	942	4.8	195		⑨	795	4.3	187
	③	1,141	8.0	143		⑩	1,045	4.0	259
	④	825	3.7	222		⑪	986	6.5	152
	⑤	945	6.1	155		⑫	793	6.4	124

and development due to the complexity of the sedimentary environments, uneven distribution of sand bodies, and changes in lithological horizons (CUI et al., 2019).

In the vertical stage, the lateral boundary of the river channel is divided mainly according to the identification mark of the configuration unit, and the boundary of the inter-well configuration unit is identified (Lu et al., 2022). In the area with a low well control degree, the lateral boundary of the river channel is reasonably divided according to the thickness of the sand body in a single river channel (ZOU et al., 2008). In the same single layer, there are still differences in the development time of multiple single braided channels in a shorter period of time, and the different development times of single braided channels in different periods will lead to

TABLE 3 Division table of configuration units.

Rank	Configuration interface classification	Stratigraphic unit	Sedimentary unit
Sequence configuration	Level 8	Segment (sub-segment)	River group
	Level 7	Small layer	Multi-stage braided channel
	Level 6	Single layer	Braided channel at the same time
Sand body configuration	Level 5	Single sand body	Single braided channel
	Level 4	Single sand body	Single microfacies
	Level 3	Rhythm layer (lithofacies combination)	Hyperplasia
Bedding configuration	Level 2	Stratification combination	Stratification series (lithofacies)
	Level 1	Lamina system	Stratification system
	Level 0	Single striation	lamina

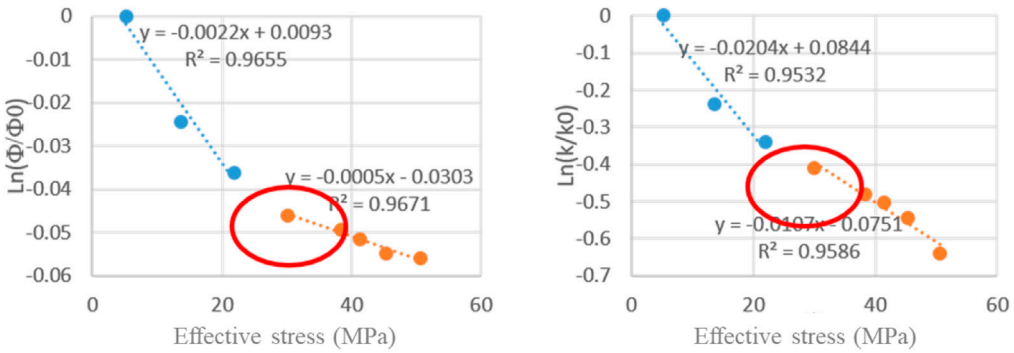

FIGURE 4
He 8 stress sensitivity results.

TABLE 4 Gas-water two-phase experiment.

Pound sign	Sample depth	Porosity (%)	Gas permeability (mD)	Permeability of the water phase (mD)	Injection pressure (Mpa)	Final gas flooding water efficiency (%)
Su 19–2	3,615.02	8.7	0.384	0.02	2.4	26.9
Su 19–4	3,615.7	7.9	0.125	0.0065	2.63	28.2
Su 19–8	3,618.44	12.1	0.092	0.005	2.48	34.8
Su 19–9	3,625.86	1.3	0.013	0.0008	3.72	9.4
Su 19–13	3,654.1	2.7	0.021	0.001	3.62	8.9
Su 19–15	3,633.31	4.3	0.033	0.002	2.72	11.9

differences in relative elevations between the top and the stratum interface, and the difference in the top elevation is an important identification sign for identifying single braided channel sand bodies. The scale difference in channel sand bodies is mainly manifested in two types: due to the lateral splicing of a single braided channel in two stages, the thin part in the middle is the edge of a braided channel sand body, or it may be due to the development of a small braided channel sand body in the middle, which is different from the braided channel sand bodies on both sides. Discontinuous inter-channel deposits develop between different single braided rivers in the same period, which indicates the boundary of a single braided river (Yang et al., 2005). The hydrodynamic intensity is often different when different braided channels are formed, which leads to the difference in logging curve response characteristics (Cheng et al., 2022). This difference can be used to identify the boundary of a single braided channel sand body. However, owing to similar differences in different parts of the same

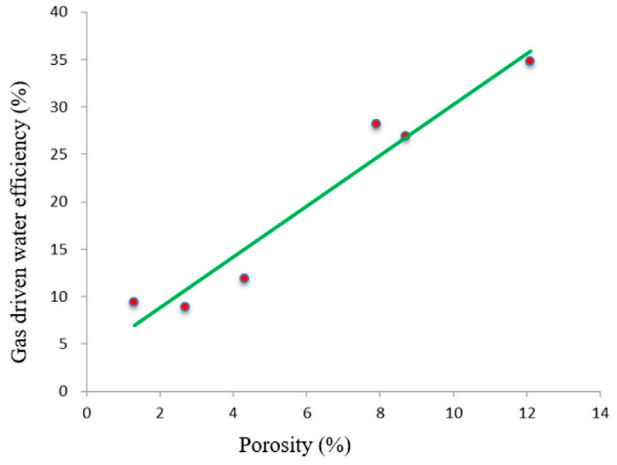

FIGURE 5
Water displacement efficiency of gas under different porosities.

configuration unit, there are multiple solutions. Therefore, when using this kind of identification mark, it should be used interactively with other plane marks.

On the basis of determining the plane distribution of the composite channel, according to the interpretation results of single well configuration elements, the position of the single braided channel on the multi-well correlation profile perpendicular to the braided channel is determined by using the single braided channel identification method (Lynds and Hajek, 2006). In this study, the single braided channel anatomy of each single layer in the lower sub-section of He 8 was carried out, and the distribution of single braided channels (five-level configuration unit) in each single layer was obtained.

Table 2 shows that the maximum sand body thickness of the single braided channel in the lower sub-section of He 8 in the study area is 1.0–8.0 m, with an average of 4.7 m, and the width of the single braided channel is 317 m–2,113 m, mainly concentrated between 700 m and 1,100 m, with an average of 963 m.

At the end of reservoir deposition, the beach is often exposed to the water, and its deposition thickness is slightly larger than that of river filling deposition at the same time. The beach is flat at the bottom and convex at the top, and the relative depth of the top surface of the beach sand body is shallower than that of the channel sand body. In this study, the relative depth of the sand body top surface is calculated using the depth difference between the single-layer top structure and the top surface structure of the sand body to identify the position of the heart beach. Based on the quantitative knowledge base constraint and the interpretation of single well configuration, the compound beach was found to be potato-shaped (Lou et al., 2023). In a single river, the long axis direction of the beach is parallel to the main flow direction, and the length of the beach is mainly between 1,600 m and 2,600 m, with an average of 2,147 m. The width of the beach is mainly between 600 m and 900 m, with an average of 844 m (Hou et al., 2019).

Based on the theoretical system of high-resolution sequence stratigraphy of Cross and the method of division and correlation, and the method of base-level cycle division of continental basin, the sequence stratigraphy of the lower member of He 8 in the field outcrop profile was divided. Table 3 shows the division of configuration units of the lower subsection of He 8.

3.2 Reservoir pore and gas-water characteristics

The reservoir pores of the Sulige gas field are mainly composed of sandstone, with high porosity and permeability, making it an

TABLE 5 Core porosity distribution.

Pound sign	Depth (m)	Average porosity (%)	Pore volume (μm^3)
Su 19–2	3,628.01	2.99	191.5
Su 19–4	3,626.6	4.76	665.343
Su 19–7	3,649.05	10.22	690.68
Su 19–9	3,763.29	5.16	584.77
Su 19–11	3,766.02	1.53	218.1

TABLE 6 Electrical values of the three-dimensional reservoir.

Pound sign	Depth (m)	X conductivity S/m	Y Conductivity S/m	Z conductivity S/m	X formation factor	Y Formation factor	Z stratum factor
Su 19–3	3,628.01	0	0.176	0.0586	+∞	569.14	1706.54
Su 19–5	3,626.6	0	0.304	0.207	+∞	328.515	483.71
Su 19–6	3,649.05	1.34	0.374	0.553	74.829	267.48	180.98
Su 19–8	3,763.29	0	0.187	0.189	+∞	535.36	528.2
Su 19–9	3,766.02	0.144	0.134	0	693.88	747.046	+∞

10.3389/fenrg.2023.1219664

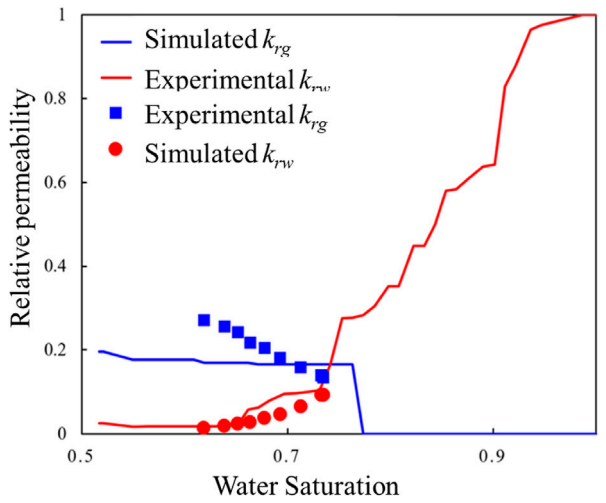

FIGURE 6
The simulation gas-water permeability and experimental results.

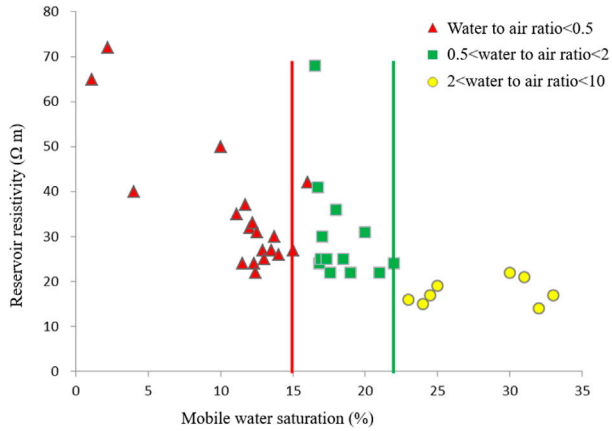

FIGURE 7
Relationship between reservoir resistivity and movable water saturation.

important reservoir space for the gas field (Tianjian et al., 2014a). It is one of the largest shale gas fields in China and is famous for its rich gas production (Bristow and Best, 1993). According to statistics, the annual gas production of the Sulige gas field can reach tens of billions of cubic meters. By contrast, its water production is usually relatively low due to the characteristics of shale reservoirs and measures taken during the mining process to reduce water production (Zheng et al., 2020).

Through the stress sensitivity test of overlying porosity and permeability, it could be concluded that the porosity stress damage rate of the reservoir core is 4.5%–5.6%, which is not obvious. When K > 1 mD, the stress damage rate of permeability is 47.9%. When 0.1 < K < 1 mD, the stress damage rate of permeability is between 22.9% and 44.6%, with an average of 30.4%. When K < 0.1mD, the stress damage rate of permeability is 26.8%–33.3%, with an average of 30.8%. Through comprehensive analysis and comparison of these data, it can be found that within the transition range of permeability from medium to low, the change in stress damage rate is relatively small and approximately 30%. As shown in Figure 4, 28 MPa was determined as the effective stress boundary point, meaning that when the *in situ* stress exceeds this value, the stress damage rate of permeability will significantly increase. According to the NMR T_2 spectrum, it can be concluded that the physical properties of reservoirs with different lithologies are quite different and the pore structure is complex. When rock granularity is smaller, the movable fluid saturation is lower and the reservoir seepage capacity is weaker (Lynds and Hajek, 2006). When the lithology is the same, the difference in porosity is small but the difference in permeability is large, and the pore structure is complex (Tianjian et al., 2014a). The collocation of pores with different sizes and throats determines the seepage size of the reservoir rock mass (Jiongxin, 1997).

Table 4 shows the gas-water two-phase experimental results. According to the experimental results, the irreducible water saturation is high (more than 50%) and the co-infiltration range is small. When the porosity is greater than 5% and the permeability is greater than 0.1 mD, certain macropores develop, the injection pressure is relatively low, and the gas drive water efficiency is greater than 20%. However, when the porosity is less than 5% and the permeability is less than 0.1 mD, small pores do not develop, the injection pressure is relatively high, and the gas flooding efficiency is less than 15%. Figure 5 shows the gas drive water efficiency under different porosities. The figure shows that with the increase in porosity, the gas drive water efficiency also increases, and there is a linear positive correlation between porosity and gas drive water efficiency.

Through CT scanning of core slices, Table 5 shows the distribution of core porosity. Table 5 shows that the average porosity of cores is small, generally ranging from 1.53% to 10.22%, but the distribution is quite different. Additionally, the distribution of void volume is relatively discrete, which has no direct relationship with porosity.

The pore structure model was imported into COMSOL Mutilphysics software for seepage simulation. Through the results of gas -water permeability simulation experiment in Figure 6, the experimental value of gas-water relative permeability was found to be quite different from the simulated value, but the overall trend of the relative permeability curve was consistent. Because of the

TABLE 7 Grading evaluation of the gas-water layer.

Gas-water layer grade	Saturation of movable water (%)	Water-gas ratio	Daily water production (m^3)
Class I	10–15	< 0.5	< 2
Class II	15–20	0.5–1.5	2–4
Class III	20–25	1.5–3	4–10

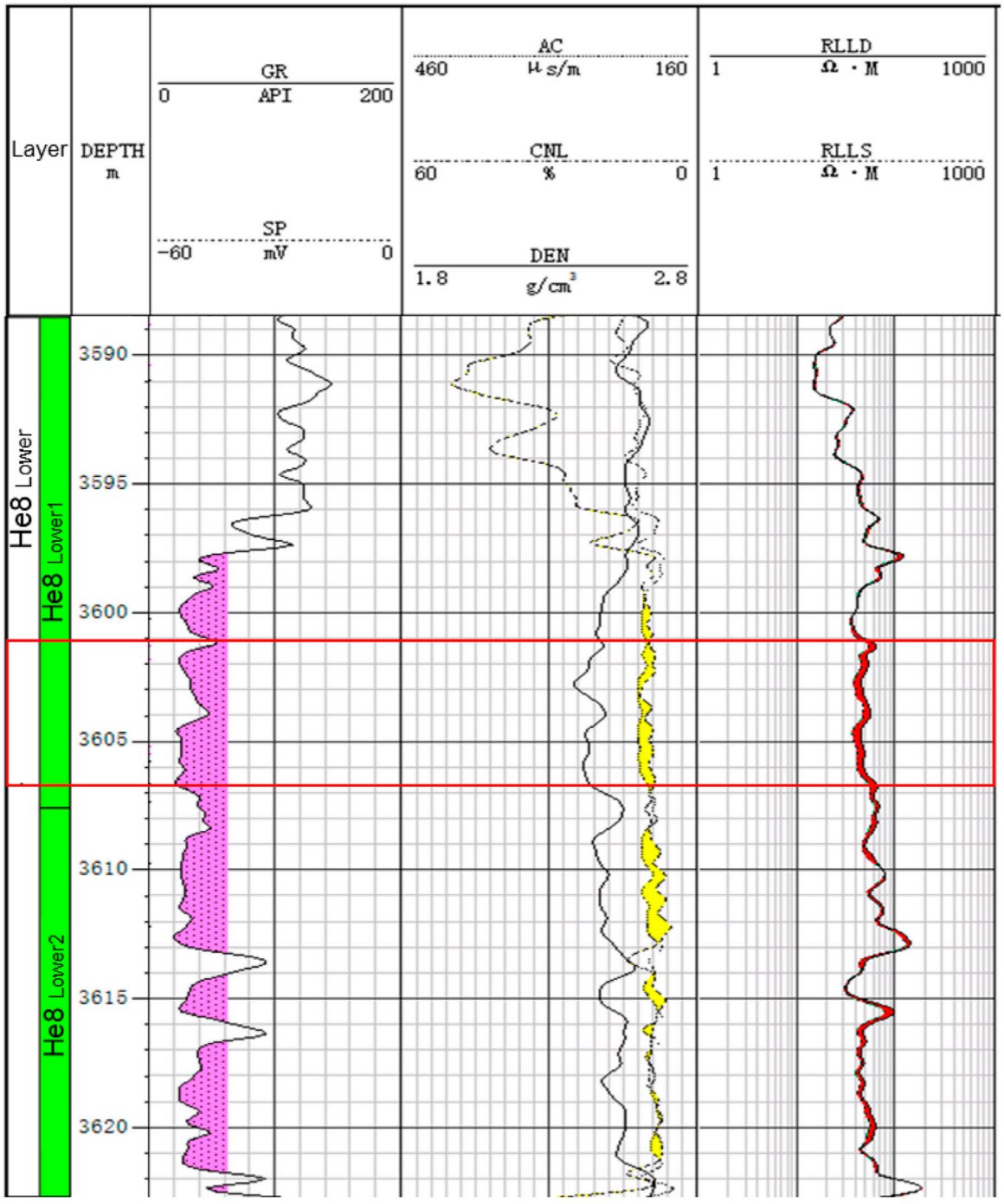

FIGURE 8
Logging curves and production of the Su 142 well.

irregular pore structure, the conductivity of the core is greatly influenced by the current direction (Wei et al., 2019). Table 6 shows the electrical properties of the three-dimensional reservoir, which demonstrate that pore connectivity and pore heterogeneity play a key role in conductivity, and under the same gas-bearing conditions, the difference in pore structure leads to the differences in electrical characteristics.

Through the comparative analysis of core resistivity and movable water saturation, the relationship between reservoir resistivity and movable water saturation is established. Figure 7 shows the relationship between reservoir resistivity and movable water saturation, from which it can be observed that when movable water saturation is less than 15%, the water-gas ratio is less than 0.6. When the movable water saturation is greater than 30%, the water-gas ratio is greater than 10. When the movable water saturation is less than 15%, as calculated by logging, the water production probability is low (generally the water production is less than 3 m^3/day). When the movable water saturation is more than

30%, the water production probability is high and the daily water production is high. With the increase in movable water saturation, the water-gas ratio becomes larger and the water production is more serious (Tianjian et al., 2014b).

Through the relationship between movable water saturation and daily water production and water-gas ratio, the gas-water layer classification evaluation was established (Table 7). According to the actual production, when the water production is low and production is high, the logging interpretation of I and II gas-water zones is gas zones.

The water-producing zones in the Sulige area are scattered in the plane, the relationship between gas and water is complicated in the vertical direction, and the water production after fracturing is different, which shows that the formation water has clearly different occurrence states (Hua and Xiuqin, 2013). According to the regional structure, reservoir pore structure, and heterogeneity, the formation water can be divided into three types: bound water, interlayer water, and local stagnant water.

Bound water is mainly adsorbed on the surface of rock particles or microcapillaries of the reservoir, which does not flow easily in the original formation state (Liu et al., 2020). Only a small amount of water is produced after fracturing, and water production is generally less than 5 m^3/d and gas production is relatively low. The reservoir cuttings and argillaceous content are high. According to the logging response in Figure 8, bound water is characterized by a medium-high time difference (220–250 μs/m) and medium-low resistivity (20–50 Ω m), which is mainly developed in tight sandstone reservoirs and has no obvious water layer logging response characteristics.

The resistivity curve changes rhythmically in a longitudinal direction, with no obvious difference between gas and water and no obvious gas-water interface. Water production of >4 m^3/d has a great influence on the interpretation of logging. In a background of low amplitude structure and low permeability, the reservoir with good local pore structure and physical properties is controlled by reservoir-forming conditions or weak structural differentiation after reservoir-forming, and the water remains at the bottom of the reservoir or sand body.

4 Conclusion

(1) The lithology of the reservoir in the study area is mainly quartz sandstone, lithic sandstone, and quartzy lithic sandstone, with a porosity of 3%–13% and a permeability of (0.05–0.7)×10^{-3} m^2, i.e., a low-porosity and low-permeability reservoir; 32 rock thin-section samples were selected by sampling boreholes. The pore types of the block reservoirs are mainly (82.9%) intragranular and intergranular dissolved pores. The difference in pore structure is mainly reflected in the size and distribution of the throat, the distribution of physical properties is 6%–10%, the gas saturation is 61%, the NMR effective porosity is 7.49%, the permeability is 4.08 × 10^2 μm^2, and the physical properties are relatively good. The average maximum sand body thickness of the single braided channel in lower section 8 is 4.7 m, and the average channel width is 963 m. The composite channel is distributed in a potato shape, parallel to the main flow direction, with an average length of 2,147 m and an average width of 844 m.

(2) As the porosity increases, the efficiency of gas-driven water also increases, and there is a linear positive correlation between porosity and gas-driven water efficiency. Under the condition of amplitude structure and a low permeability background, for reservoirs with better local pore structure and physical properties, the water remaining in the bottom of reservoirs or sand bodies is controlled by accumulation conditions or weak structural differentiation after accumulation. When water is produced at the same time, water production is relatively large at more than 10 m^3/d, and gas production is less than 2 × 10^4 m^3/d; the water and gas are mainly distributed in the downdip part of the main channel structure or the island lens-shaped permeable sand bodies trapped by the surrounding tight layers in the middle.

Data availability statement

The original contributions presented in the study are included in the article/Supplementary Material, further inquiries can be directed to the corresponding author.

Author contributions

ZH, MH, XX, LZ, NW, YG, XaH, and XnH contributed to conception and design of the study. ZH, MH, and XX organized the database. LZ, NW, YG, XaH and XnH performed the statistical analysis. ZH, MH, XX, LZ, NW, YG, XaH, and XnH wrote the first draft of the manuscript. ZH, MH, XX, and LZ wrote sections of the manuscript. All authors contributed to the article and approved the submitted version.

Funding

This work was supported by the Distribution and evolution of overpressure in the Ordovician, eastern Ordos basin (Project No. 42172179).

Acknowledgments

The authors would like to express their sincere thanks for those techniques that have contributed to this research.

Conflict of interest

Authors ZH, LZ, YG, and XaH were employed by the company Geological Research Institute of CNPC Xibu Drilling Engineering Company Limited. Author XX was employed by the company PetroChina Coalbed Methane Company Limited.

The remaining authors declare that the research was conducted in the absence of any commercial or financial relationships that could be construed as a potential conflict of interest.

Publisher's note

References

Bristow, C. S., and Best, J. L. (1993). Braided rivers: perspectives and problems. *Geol. Soc. Lond. Spec. Publ.* 75 (1), 1–11. doi:10.1144/gsl.sp.1993.075.01.01

Caili, Z. H. A. N. G., Xinshe, L. I. U., Yajuan, Y. A. N. G., Jian, Y. U., Tianyou, H. A. N., and Yan, Z. H. A. N. G. (2021). Petroleum exploration history and enlightenment of changqing oilfield in Ordos Basin. *Xinjiang Pet. Geol.* 42, 17. doi:10.7657/XJPG20210301

Cheng, H., Ma, P., Dong, G., Zhang, S., Wei, J., and Qin, Q. (2022). Characteristics of carboniferous volcanic reservoirs in beisantai oilfield, junggar basin. *Math. Problems Eng.* 2022, 1–10. doi:10.1155/2022/7800630

Cui, M., Fan, A., Wang, Z., Gao, W., Li, J., and Li, Y. (2019). A volumetric model for evaluating tight sandstone gas reserves in the Permian Sulige gas field, Ordos Basin, Central China. *Acta Geol. Sinica-English Ed.* 93 (2), 386–399. doi:10.1111/1755-6724.13811

Hou, Z. K., Cheng, H. L., Sun, S. W., Chen, J., Qi, D. Q., and Liu, Z. B. (2019). Crack propagation and hydraulic fracturing in different lithologies. *Appl. Geophys.* 16 (2), 243–251. doi:10.1007/s11770-019-0764-3

Hua, Y., and Xiuqin, D. (2013). Deposition of Yanchang Formation deep-water sandstone under the control of tectonic events in the Ordos Basin. *Petroleum Explor. Dev.* 40 (5), 549–557. doi:10.1016/s1876-3804(13)60072-5

Jiongxin, X. (1997). Evolution of mid-channel bars in a braided river and complex response to reservoir construction: an example from the middle hanjiang river, China. *Earth Surf. Process. Landforms J. Br. Geomorphol. Group* 22 (10), 953–965. doi:10.1002/(sici)1096-9837(199710)22:10<953::aid-esp789>3.0.co;2-s

Li, G., Qin, Y., Shen, J., Wu, M., Li, C., Wei, K., et al. (2019). Geochemical characteristics of tight sandstone gas and hydrocarbon charging history of Linxing area in Ordos Basin, China. *J. Petroleum Sci. Eng.* 177, 198–207. doi:10.1016/j.petrol.2019.02.023

Li, J., Zhang, X., Tian, J., Liang, Q., and Cao, T. (2021). Effects of deposition and diagenesis on sandstone reservoir quality: a case study of permian sandstones formed in a braided river sedimentary system, northern Ordos Basin, northern China. *J. Asian Earth Sci.* 213, 104745. doi:10.1016/j.jseaes.2021.104745

Liu, Y., Xian, C., Li, Z., Wang, J., and Ren, F. (2020). A new classification system of lithic-rich tight sandstone and its application to diagnosis high-quality reservoirs. *Adv. Geo-Energy Res.* 4 (3), 286–295. doi:10.46690/ager.2020.03.06

Lou, T., Feng, C., Sun, M., and Chen, Z. (2023). The upper triassic braided river thin-bedded tight sandstone in the Yanchang formation, ordos basin: sedimentary characteristics, seismic forecasting method, and implication. *Processes* 11 (5), 1303. doi:10.3390/pr11051303

Lu, T., Liu, Y., Wu, L., and Wang, X. (2015). Challenges to and countermeasures for the production stabilization of tight sandstone gas reservoirs of the Sulige Gasfield, Ordos Basin. *Nat. Gas. Ind. B* 2 (4), 323–333. doi:10.1016/j.ngib.2015.09.005

Lu, Z., He, Z., Ma, S., and He, Y. (2022). Sedimentary characteristics and sand-body distributions in the lower permian He-8 member, Ordos Basin, China. *Interpretation* 10 (2), T223–T236. doi:10.1190/int-2021-0101.1

Lynds, R., and Hajek, E. (2006). Conceptual model for predicting mudstone dimensions in sandy braided-river reservoirs. *AAPG bull.* 90 (8), 1273–1288. doi:10.1306/03080605051

Tianjian, S., Longxin, M., and Guoliang, Z. (2014a). Classification and characterization of barrier-intercalation in sandy braided river reservoirs: taking Hegli Oilfield of Muglad Basin in Sudan as an example. *Petroleum Explor. Dev.* 41 (1), 125–134. doi:10.1016/s1876-3804(14)60015-x

Tianjian, S., Longxin, M., Xianghong, W., Guoliang, Z., Feng, X., Zhenjun, W., and Ziqi, F. (2014b). A quantitative method for architectural characterization of sandy braided-river reservoirs: taking hegli oilfield of muglad basin in Sudan as an example. *Acta Pet. Sin.* 35 (4), 715. doi:10.7623/syxb201404012

Wei, X., Guo, Y., Cheng, H., Meng, X., Cheng, M., Yang, T., et al. (2019). Rock mass characteristics in beishan, a preselected area for China's high-level radioactive waste disposal. *Acta Geol. Sin.* 93 (2), 362–372. doi:10.1111/1755-6724.13766

Yang, H., Fu, J., Wei, X., and Liu, X. (2008). Sulige field in the Ordos Basin: geological setting, field discovery and tight gas reservoirs. *Mar. Petroleum Geol.* 25 (4-5), 387–400. doi:10.1016/j.marpetgeo.2008.01.007

Yang, Y., Li, W., and Ma, L. (2005). Tectonic and stratigraphic controls of hydrocarbon systems in the Ordos basin: a multicycle cratonic basin in central China. *AAPG Bull.* 89 (2), 255–269. doi:10.1306/10070404027

Zheng, M., Tang, H., Li, H., Zheng, J., and Jing, C. (2020). Geomechanical analysis for deep shale gas exploration wells in the NDNR blocks, sichuan basin, southwest China. *Energies* 13 (5), 1117. doi:10.3390/en13051117

Zhu, H., Huang, C., Ju, Y., Bu, H., Li, X., Yang, M., et al. (2021). Multi-scale multi-dimensional characterization of clay-hosted pore networks of shale using FIBSEM, TEM, and X-ray micro-tomography: implications for methane storage and migration. *Appl. Clay Sci.* 213, 106239. doi:10.1016/j.clay.2021.106239

Zhu, H., Ju, Y., Qi, Y., Huang, C., and Zhang, L. (2018). Impact of tectonism on pore type and pore structure evolution in organic-rich shale: implications for gas storage and migration pathways in naturally deformed rocks. *Fuel* 228, 272–289. doi:10.1016/j.fuel.2018.04.137

Zhu, P., Meng, X., Wang, X., Dong, Y., Li, X., Zhang, C., et al. (2022). Geochemical characteristics of diagenetic fluid and densification model of tight gas sandstone reservoirs in Linxing area, eastern margin of Ordos Basin, China. *Mar. Petroleum Geol.* 138, 105496. doi:10.1016/j.marpetgeo.2021.105496

Zou, C. N., Tao, S. Z., Hui, Z., Zhang, X. X., He, D. B., Zhou, C. M., et al. (2008). Genesis, classification, and evaluation method of diagenetic facies. *Petroleum Explor. Dev.* 35 (5), 526–540. doi:10.1016/s1876-3804(09)60086-0